Journal of Materials Chemistry B

Accepted Manuscript

ROYAL SOCIETY OF CHEMISTRY

www.rsc.org/materialsB

Journal of

Material Chemistry B

ARTICLE

Tuning Glyconanomaterial Shape and Size for Selective Bacterial Cell Agglutination

Received 00th January 20xx,
Accepted 00th January 20xx

DOI: 10.1002/x0xx00000x

www.rsc.org/

J-J. Cid Martín, [a] M. Assali,[a] E. Fernández-García,[b] V. Valdivia,[a,c] E. M. Sánchez-Fernández, [d] J. M. Garcia Fernández,[a] R-E. Welinger,[b] I. Fernández, [c] and N. Khiar*[a]

Multivalent glycosystems are potential candidates for anti-adhesive therapy, a non-lethal approach against the ever increasing antibiotic resistance of pathogenic bacteria. In order to fine tune the glyconanomaterials size and shape for selective bacterial cell agglutination, herein we report the synthesis of sugar-coated dynamic and polymeric 3D-micelles and 1D-carbon nanotubes. The reported shot-gun like synthetic approach is based on the ability of diacetylenic-based neoglycolipids to self-assemble into micelles in water and to hierarchically self-assemble in hemimicelles on single-walled carbon nanotube surface. The affinity of the nanosystems was preliminary assessed by enzyme-linked lectin assay (ELLA) using the mannose-specific Concanavalin A lectin as a model receptor. Relative binding potency enhancements, compared to methyl α-D-mannopyranoside used as control, from 10-, to 25- to 975-folds in sugar molar basis were observed when passing from 3D dynamic micelle to static micelle, to 1D-mannose coated carbon nanotubes, respectively, ,indicative of a significant cluster glycoside effect. Importantly, these results were confirmed *in vivo* showing that the 1D-glyconanoring-coated carbon nanotubes efficiently and selectively regulate the agglutination and proliferation of the enterobacteria *Escherichia coli* type 1 fimbriae. These findings highlight the potential of sugar coated nano-materials as novel and effective tools in the control of bacterial pathogenesis.

1 Introduction.

The relevance of the physiological and pathological processes involving carbohydrates has put research on glycobiology in the frontline of pharmaceutical and medical research.[1] Interactions between carbohydrate ligands and carbohydrate binding proteins (lectins) are at the origin of fertilization, immune response, cell adhesion and tumor cell metastasis, among others.[2] Many infections by pathogens and toxins, including some of the most virulent and dangerous viruses, are also mediated by carbohydrate-lectin intercations. For instance, influenza virus displays hemagglutinins (sialic acid binding lectins) for adhesion to target cells,[3] while HIV[4] and Ebola[5] viruses express high-mannose chain glycoproteins that are able to bind a C-type lectin (DC-SIGN) on immune cell populations that are predominantly comprised of dendritic cells.[6] In addition, carbohydrates play an important role in the early stages of cell infection by pathogenic bacteria through specific lectins, the so-called adhesins.[7] Synthetic compounds blocking these adhesins have the potential to inhibit the adherence of bacteria to epithelial cell walls, preventing infection. This strategy, so-called anti-adherent therapy,[8] is particularly relevant as a possible alternative to antibiotics that are prone to bacterial resistance.[9] Because lectin blockers are generally not internalized, it is less likely that the bacteria develop resistance against them. Even assuming that this would be the case, the bacteria would possibly lose their ability to adhere to the cell surface and therefore, their virulence.

The development of an anti-adhesive therapy has been hampered because the structure of the majority of functional carbohydrates remains unknown and high structural complexity of known carbohydrates structures constrains their synthesis.[10] In addition, adhesin- and in general protein-carbohydrate interactions are characterized by low affinity (usually in the millimolar range), high affinity interactions in nature being achieved by organizing carbohydrates as multivalent structures or glycoclusters.[11] Therefore, synthetic multivalent surrogates for the adequate recognition of carbohydrate receptors based on the so called "cluster glycoside effect"[12] would be a major advance in the development of anti-adherent therapies.

Given the accessibility and facility in functionalizing scaffolds such as metal nanoparticles, dendrimers, calixarenes, fullerenes, and cyclodextrins, the majority of the multivalent

[a] *Asymmetric Synthesis and Functional Nanosystems Group. Instituto de Investigaciones Químicas (IIQ), CSIC and Universidad de Sevilla, C/ Américo Vespucio 49, 41092, Seville (Spain). E-mail: khiar@iiq.csic.es*
[b] *Miochondrial Plasticity and Replication Laboratory. Andalusian Center for Molecular Biology and Regenerative Medicine (CABIMER), Av. Americo Vespucio s/n, 41092, Seville (Spain).*
[c] *Departamento de Química Orgánica y Farmacéutica, Universidad de Sevilla, C/ García González 2, 41012 Seville (Spain).*
[d] *Departamento de Química Orgánica, Universidad de Sevilla, Facultad de Química, 41012 Seville, Spain.*

†Electronic Supplementary Information (ESI) available: [Experimental procedures for the synthesis of compound **2**, NMR spectrum of **2**, Synthesis of **NP3** Fluorescence CMC determination, UV-Vis-NIR spectra, Anthrone Method, TGA and Fluorescence microscopy]. See DOI: 10.1002/x0xx00000x

systems obtained so far have spherical shapes.[13] Recent studies have shown that the geometry of glycocoated nanosystems has a significant impact on their abilities to generate networks, and to interact with specific lectins present in biological membranes.[14] Thus, synthetic designs allowing the divergent synthesis of functionalized multivalent nanosystems with varied morphologies, preferentially from a common intermediate, with no additional synthetic cost are therefore highly desirable.[15] The sequential approach -ligating monomeric or block species in a step-wise manner- usually followed is highly challenging, time consuming and clearly not suitable for this enterprise.

Supramolecular self-assembly mediated by non-covalent forces, such as hydrogen bonding, π–π stacking, electrostatic and charge-transfer interactions,[15] is the most appropriate approximation to induce self-assembling glyco-monomers into multivalent systems with diverse topology, composition, and assembly dynamics.[16] Such multivalent systems may then be further manipulated in the supramolecular state in order to endow the glyconanomaterials with the needed physicochemical stability.

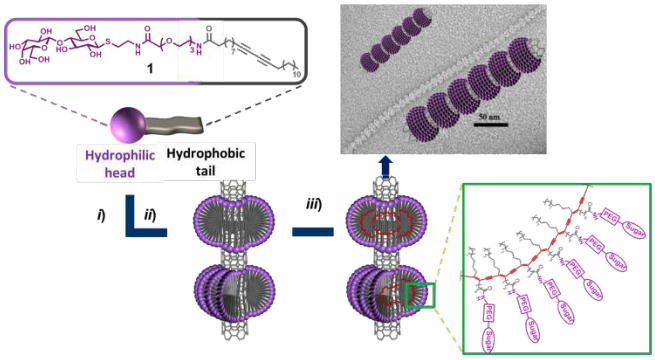

Figure 1. Procedure for SWCNT/**1** nanoassembly formation (A) *i*)) Sonication-promoted supramolecular self-assembly of neoglycolipid **1** in concentric hemi-micelles around SWCNTs in water. *iii*) Intermolecular photo-polymerization of neoglycolipid **1** hemi-micelles into homogeneous glyconanorings (GNRs). Above, TEM micrograph of SWCNT/**1** nanoassemblies.

Diacetylenic amphiphiles are well suited for the above endeavour as they can undergo, upon UV-irradiation or thermal stimuli, a clean photo-polymerization *via* a 1,4-addition reaction, affording functional polydiacetylene (PDA)-nanomaterials with enhanced stability and interesting chromatic properties.[17] Accordingly, we have recently reported that lactose-based neoglycolipid **1** was capable of self-assembled on single wall carbon nantube (SWCNT)[18] surfaces in a supramolecular fashion, resulting in rings made of rolled-up half cylinders (Figure 1, step *i*). Photo-polymerization of the diacetylene function upon ultraviolet irradiation (254 nm) afforded a conjugated polydiacetylene backbone of alternating enyne groups (step *ii*) which rigidified the inner core of each hemi-micelle, resulting in robust polymerized glyconanorings (GNRs) around the nanotube in an abacus-like geometry.[19]

Further studies unraveled that neoglycolipid **1** first self-organizes into micelles in aqueous solution, and then undergo a hemi-micellar arrangement on the solid surface of the SWCNTs.[20] Interestingly, we found that both micelles and glyconanotubes are multivalent systems exposing a large number of carbohydrate ligands on their surface. Moreover, the three-dimensional structure of the micelles and monodimensional structure of glyconanotubes offer an excellent opportunity to study the topology significance on the cluster glycoside effect at the nanoscale.[21]

Here we report the synthesis of mannose-coated dynamic and static micelles from diacetylene-derived mannopyranosyl glycolipids. In the presence of single walled carbon nanotubes (SWCNTs), the dynamic micelles hierarchically self-assemble onto the nanotube surface in form of rings made of rolled-up half cylinders, affording stable water soluble 1D-nanoconstructs. The structure and shape of the 3D and 1D-nanomaterials produced have been investigated by nuclear magnetic resonance (NMR), near infrared spectroscopy (NIR), transmission electron microscopy (TEM), atomic force microscopy (AFM), dynamic light scattering (DLS), and Raman spectroscopy. The sugar content in the neoglycolipid aggregates and in the mannosyl-coated SWCNT has been determined by the anthrone method and by thermogravimetric analysis. Finally, we determined the ability of the new glyconanomaterials to specifically interact with lectins by the so-called Enzyme-linked Lectin Assay (ELLA). Using the mannose-specific lectin Concanavalin A, strong glycoside cluster effects were observed, demonstrating the availability of the sugar epitopes at the surface of micelles and carbon nanotubes to participate in multivalent molecular recognition processes. To validate these observations *in vivo*, we verified the potency and selectivity of these nanomaterials to aggregate the enterobacteria *Escherichia coli* (*E. coli*) type 1 fimbriae (Figure 2). Taken together, we report a proof-of-principle for the use of supramolecular glyconanomaterials as a tool for anti-adhesive therapies.

2. Results and discussion

2.1 Chemistry

2.1.1. Synthesis and characterization of mannose-coated 3D-glyconanomicelles (NP1 and NP2)

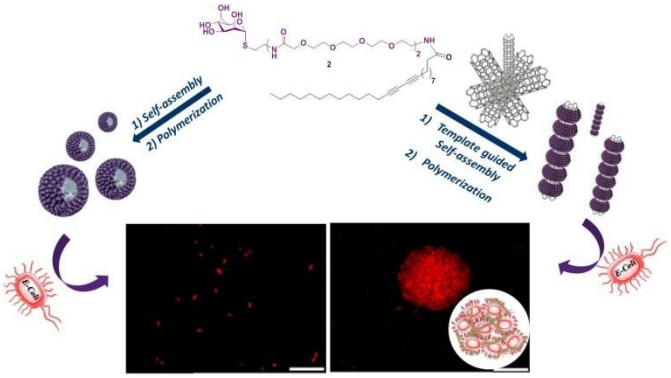

Figure 2: Short-gun convergent synthesis of multivalent mannose-coated 3D-micelles and 1D-glyconanotubes used for the regulation of bacterial cells agglutination (Scale bars, 10µm).

Binding of multivalent mannose constructs to the plant lectin Concanavalin A (ConA) has been profusely studied, providing an excellent model to test the performace of the newly synthesized mannose coated nanomicelles and glyconanotubes in molecular recognition events.[22] Moreover, multivalent mannosides are able to specifically aggregate uropathogenic fimbriated bacteria by interacting with FimH lectin, which allows further probing the influence of variations in the geometrical parameters of the glyconanosystems in a model of therapeutic interest.[23] For the purpose of this work, we have chosen to work with neoglycolipid **2** having a mannose head group, a long ethyleneglycol chain and a 25 carbon-based fatty acid containing a photopolymerizable diyne function (Scheme 1).

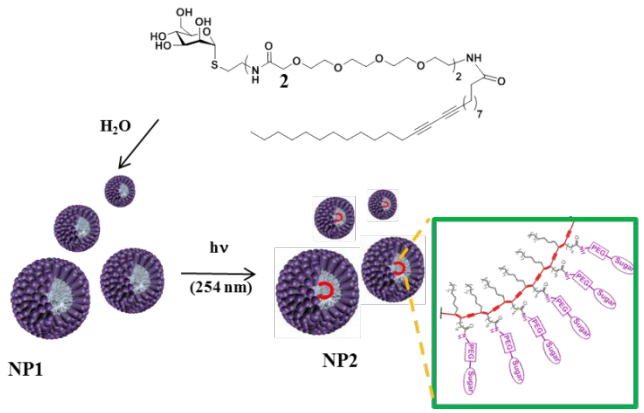

Scheme 1. Procedure the synthesis of dynamic (NP1) and static (NP2) mannose-coated nanomicelles *i*)) Sonication-promoted supramolecular self-assembly of neoglycolipid 2 into micelles in water. *ii*) Intermolecular photo-polymerization of neoglycolipid 2 into homogeneous static micelles (NP2).

Neoglycolipid **2** was obtained in four steps starting from 2-aminoethyl 2,3,4,6-tetra-*O*-acetyl-α-D-thiomanopyranoside[19a] and fully characterized (see SI). The amphiphilic neoglycolipid **2** showed a critical micellar concentration (CMC) in water of 2.78 µM as determined by fluorescence using pyrene as a probe.[24] Formation of the nanomicellar system **NP1** was carried out by a simple dispersion of the neoglycolipid **2** in water at a concentration above the CMC. The photo-polymerization of the diacetylene function upon ultraviolet irradiation (254 nm) afforded a conjugated polydiacetylene backbone of alternating enyne groups (Scheme 1), which rigidified the inner core of the micelles resulting in robust polymerized micelles, **NP2**.

The characteristic size and morphology of nanomicelles **NP1** and polymerized nanomicelles **NP2** were determined by DLS and TEM. The size distribution histogram of the non-polymerized micelles **NP1** in aqueous solution gives a multimodal distribution with a hydrodynamic diameter of 8.25 nm and a narrow polydispersion with a polydispersion index (PDI) of 0.17 (Figure 3A). The static micelles **NP2** (Figure 3B) were also obtained with narrow polydispersity (PDI = 0.10), and with a small change in the hydrodynamic diameter (7.2 nm), as a consequence of shrinking caused by the photopolymerization. The morphology of the supramolecular 3D-micelles visualized by TEM is shown in Fig. 3C and 3D. The neoglycolipid self-assembles in aqueous solution into spherical micelles with a diameter similar of that obtained with DLS measurements. Interestingly, these results also indicate that the size of self-assembled micelles derived from neoglycolipid **2** suits the size of nanomaterials currently used as nanovectors for intracellular drug delivery.

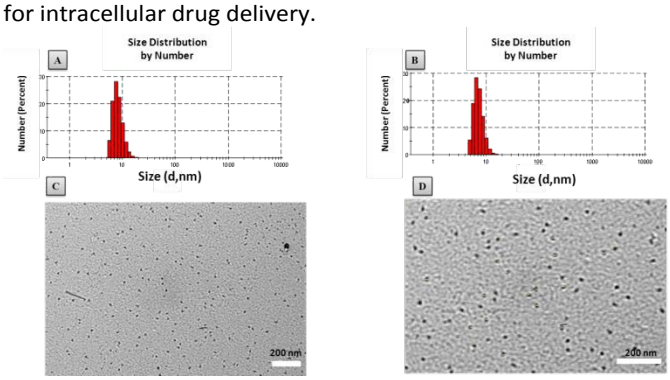

Figure 3. Micelle's size determination. Representative size distribution of no-polymerized, **NP1** (A) and polymerized micelle, **NP2** (B) determined by DLS. Representative TEM images of no-polymerized, **NP1** (C) and polymerized micelle, **NP2** (D)

2.1.2 Synthesis and characterization of mannose-coated SWCNTs (1D-glyconanotubes, NP3)

Next, we synthesized 1D-mannose-coated SWCNTs following our recently reported mixed covalent/non-covalent functionalization of carbon nanotubes.[25] Briefly, after sonication (30 min) of SWCNTs (1 mg) in the presence of an aqueous solution of lipid **2** (1 mg), the mixture was irradiated by a simple laboratory UV lamp (254 nm) for 12 h. A series of successive centrifugations allowed the elimination of excess of nanotube lipid micelles and other impurities such as amorphous carbon and catalysts.

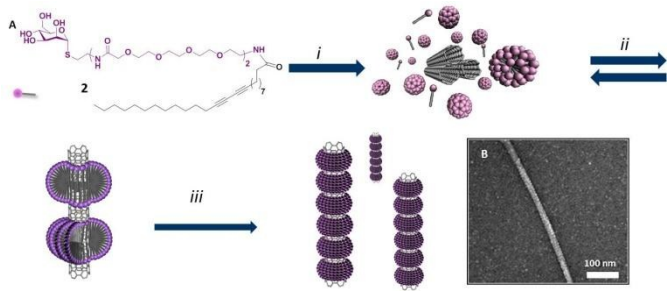

Scheme 2. Procedure for the synthesis of SWCNT/**2** (**NP3**) nano-assembly. (A) *i*) Mix of neoglycolipid **2** at its critical micelle concentration in water with SWCNTs. *ii*) Sonication-promoted supramolecular self-assembly of neoglycolipid **2** in concentric hemi-micelles around SWCNTs. *iii*) Intermolecular photo-polymerization of neoglycolipid **1** hemi-micelles into homogeneous glyconanorings-coated carbon nanotubes. (B) TEM micrograph of SWCNT/**2** nanoassemblies

The obtained nanomaterial **NP3** was highly stable in water and in physiological medium, presenting an interesting biocompatibility profile. The corresponding UV-Vis/NIR absorbance spectrum was indicative of good dispertion and preservation of the electronic structure of the carbon nanotubes. Raman spectroscopy confirmed the absence of defects on the aromatic structure of the carbon nanotubes, supporting that the nanotube surface is totally roofed by the neoglycolipid.[25] TEM images (Scheme 2B) show striations that covered the complete surface of the nanotube in a similar way to that of pearls on an open necklace.

Quantification of the carbohydrate content in the nanomaterial **NP3** was determined by spectrophotometry using the anthrone method.[26] A 15±1% of D-mannose was found in the hybrid nanomaterial SWCNTs-**2**, thus indicating a total percentage of 88±5% (0.83 mmol/g) of the corresponding glycolipid. Additionally we studied the weight loss by thermogravimetric analysis (TGA). The percentage mass loss for SWNTs-**2** at 600 °C (under a stream of N_2 at a heating rate of 20°C / min) was 52%. This loss is correlated with the stability of the starting glycolipid **2** at 600 °C, for which the decrease in mass was 60%. Given these values, the total mass loss was estimated to 86±5% for glycolipids **2**, in agreement with the anthrone result.

2.2. Quantification of the multivalent binding of mannose-coated 3D-micelles and 1D-glyconanotubes

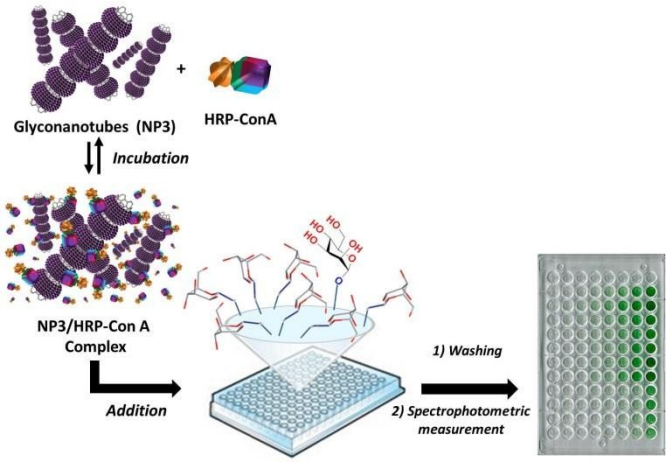

Figure 4. Schematic representation of ELLA used for the quantification of ConA HRP-to-mannan binding in the presence of **NP3**.

Binding of multivalent mannose constructs to the plant lectin Concanavalin A (ConA) is well studied and provides an excellent model to test the performance of the newly synthesize mannose coated glyconanomicelles and nanotubes in molecular recognition events.[22] For example, mannose-coated polyvalent structures are known to competitively inhibit Concavalin A (ConA) binding to yeast mannan.[26] ConA is a lectin obtained from jack bean (*Concavalis ensiformis*) known to selectively recognize α-mannopyranoside, α-glucopyranoside and to a lesser extent α-*N*-acetylglucosamine motifs, but not β-pyranosides.[27] The ConA monomer is a 26 kDa protein with one carbohydrate binding site. In the pH range of 5.0-5.6, ConA exists as a dimer, whereas at higher pH of 7.4 ConA dimer associate into tetramer containing four spatially well separated binding sites (6.5 nm) for oligosaccharides.[28] The molecular recognition of mannose-coated diacetylenic lipid **2** self-assembled into multivalent micelles (**NP1** and **NP2**) and hierarchically self-assembled in hemi-micelles onto the nanotube surface (**NP3**) were analyzed by using an enzyme-linked lectin assay (ELLA).[29] Experiments using horseradish peroxidase labelled concanavalin A (ConA-HRP) as the lectin and yeast mannan as the immobilized polymeric ligand were performed in 96-well plates as illustrated in Figure 4.

After pre-incubation of ConA-HRP with different concentrations of non-polymerized micelles **NP1**, polymerized micelles **NP2**, mannose coated 1D-nanotube **NP3**, or methyl α-D-mannopyranoside as monovalent reference compound, binding of ConA-HRP to mannan-coated plates was measured (Figure 5). The ConA-HPR activity converts a pro-dye substrate into a green dye, whose intensity is proportional to the concentration of retained lectin and inversely proportional to the affinity of the (multivalent) ligand towards the lectin. As shown in Figure 5A, **NP1-NP3** binding to ConA-HRP inhibits attachement of the later to mannan in the well, decreasing conversion of the pro-dye substrate and allowing determining the half-maximal inhibitory concentration (IC_{50}) of each glyconanoparticle (Figure 5).

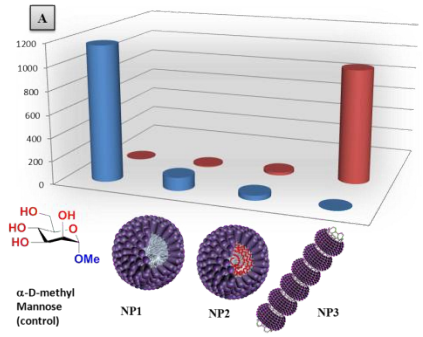

B

	IC_{50} (μM)	Rel. Potency
MeMan (Control)	1170	1
NP1	113	10
NP2	46	25
NP3	0.5	2340

Figure 5. Inhibition of ConA-HRP binding with **NP1-NP3**. Graphical (A) and table (B) showing the IC_{50} (blue) and the potency (red) relative to the monovalent control methyl α-D-mannopyranoside of the nanoparticles **NP1**-**NP3** in inhibiting ConA-HRP binding to yeast mannan.

The IC_{50} value of methyl α-D-mannopyranoside in our assay was 1170 μM, which is in agreement with values reported in the literature.[30] Both, the non-polymerized **NP1** and polymerized micelles **NP2**, as well as the glyconanotube **NP3** showed a much higher affinity for the lectin than the monovalent mannose control. The 3D-dynamic micelles **NP1** dispalyed an IC_{50} of 113 μM, meaning one order of magnitude higher lectin binding potency as compared with methyl α-D-mannopyranoside, in spite of the intrinsically monovalent nature of the constitutive neoglycolipid **2**. Taking into account the size of micelles (8.2 nm diameters) and the distance between two mannose bindings site in the Con A (6.5 nm), the enhanced affinity may be ascribed either to a chelate effect or to a statistical rebinding.[31] Potency further more than doubled for the static micelle **NP2** (IC_{50} 46 μM) compared to the dynamic micelle **NP1**, which can be ascribed to the higher stability of the static constructs, with optimized presentation of the mannosyl motifs. Impressively, the IC_{50} of the 1D-glyconanotube **NP3** was only 0.5 μM, which represents one of the best binders to ConA reported to date. For comparison, an IC_{50} of 9 μM has been recently reported for mannose-coated nanodiamonds in the same experimental setup.[32] The more than three-order-of-magnitude higher potency of the glyconanotube compared to the monovalent ligand, in a mannose molar basis, is probably the result of a chelate effect associated with bind and slid mechanism.[33] On the other hand, the practically 100 times better performance of monodimensional **NP3** compared to 3D **NP2** is a clear indication on the importance of the 1D-nanosystem topology and its flexibility, which allow both the interaction of mannose ligands with multiple binding site of Con A, and the internal diffusion of the lectin along the glyconanotube surface. In control experiments, micelles and SWCNT-aggregates obtained from lactosyl glycolipid **1**, showed no affinity for the lectin in agreement with the known specificity of Con A (see SI).

It is worth highlighting at this point the simplicity of the methodology developed for synthesizing and modulating the biological activity of these multivalent systems. Mixing compound **2** in water at a concentration higher than its CMC directly affords **NP1** with ten-fold enhanced affinity toward ConA compared with the reference monovalent ligand methyl α-D-mannopyranoside. In situ polymerization of **NP1** system to give **NP2** allows a further increase in the affinity up to 45 times. Taking into account that the polymerization process takes place without a catalyst or initiator, there is no need of an extra step for purifying nanoparticle **NP2**. Repeating the same process that led to **NP2** in the presence of SWCNTs gives rise to **NP3** system, which is thousand times more efficient than the monovalent control to bind Con A, and as such one of the best binders reported to date. These synthetic benefits greatly facilitate the optimization of other important parameters such as the control of the number of epitopes and the distance between them, in order to develop effective multivalent systems.

2.3. Selective agglutination of *E. coli* type 1 fimbriae by NP3

The adhesion of uro-pathogenic, fimbriated bacteria to the mannose moieties of glycosylated cell wall proteins provides another model system to study mannose-lectin interactions in bacteria of therapeutic interest.[23] Type 1 fimbriae are adherence factors encoded by the chromosomally located fim gene cluster (FimA-FimH) in *E. coli*.[34] FimH recognizes terminally located D-mannose moieties on cell- bound and secreted glycoproteins,[35] and is the receptor responsible of the specific binding of the bacteria to mannosylated glycoproteins in the bladder epithelium.[36] We were interested in examining the ability of our glyconanosystems **NP1**, **NP2** and **NP3** to recognize and specifically aggregate bacteria, thereby preventing attachment to the cells (Figure 6).

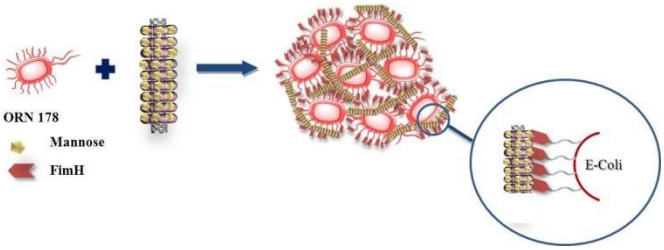

Figure 6. Schematic representation of the Fim H adhesin promoted specific interaction of *E.coli* with **NP3**.

For that purpose, *E. coli* strains ORN178 (forming α-mannose interacting type 1 pili) and ORN208 (lacking the mannose receptor FimH),[37] were first transformed with the red-fluorescent mCHERRY-protein expressing plasmid pGEM-T. *E. coli*–**NP** interactions were then followed by fluorescence microscopy. To avoid unspecific interaction with the growth medium, exponentially grown *E. coli* were diluted in phosphate-buffered saline (PBS) solution prior to a 2 h incubation period in the presence of **NP1**, **NP2** or **NP3**. While micelles **NP1** and **NP2** barely induced the formation of *E. coli* aggregates (Figure 7A, and 7B), **NP3** induced the formation of giant *E. coli*-**NP3** clusters upon incubation with FimH-presenting ORN178 bacteria, but not in the case of the FimH-devoid ORN208 strain (Figure 7A, bottom). These findings suggest that the aggregation process relies in specific mannose-FimH lectin interactions and that the size and

topology of the mannose-coated nanoparticles play an important role in the agglutination of bacterial cells. In the case of the glyco-SWCNTs **NP3**, the interaction of the exposed mannose residues with FimH receptors on the bacterial surface seemed to be extremely efficient at clusterizing *E. coli* in the form of a "fireball" formed by thousands of bacteria.

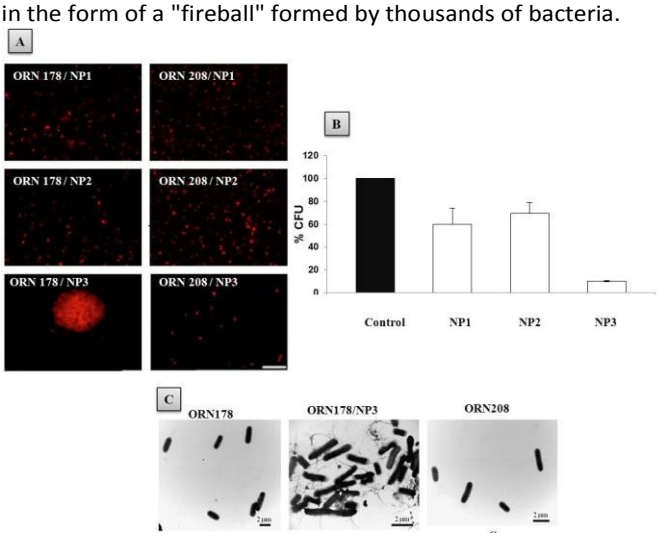

Figure 7. Selective interaction of **NP3** with *E.coli* strain ORN178 (A) Representative fluorescence microscopy images of *E.coli* strains ORN178 and ORN 208 with **NP1**, **NP2** and **NP3** (Scale bars, 10μm). (B) Colony forming units (CPU) assay. The number of colonies formed in the absence (control) and presence of **NP1, NP2**, and **NP3** for ORN178 cells is indicated. Representative TEM images of *E.coli* strains ORN178 and ORN 208 alones, and ORN178 with **NP3**. For conditions see text and Materials and Methods. Size bars are shown.

The interaction of **NP3** with *E. coli* was further characterized by high resolution TEM analysis (Figure 7C). The TEM image permits a closer look at ORN178-**NP3** aggregate, showing that the bacteria were entangled by the mannose coated nanotubes in a spider web-like morphology. In contrast, ORN208 did not interact with **NP3** and these bacteria remained dispersed. Control experiments using the previously reported carbon nanotubes coated with lactose, which is not a ligand of FimH, instead of **NP3** showed no formation of bacteria aggregates with either ORN178 or ORN208. These results further support the idea that glyconanotube **NP3** binds to bacteria through a selective mannose-FimH receptor interaction.

Uncontrolled bacterial proliferation is an important threat to human health leading to inflammation and activation of the immune system. Previous studies have linked bacterial aggregation to a repression of bacterial growth,[38] and we therefore anticipated that **NP3** could be a suitable inhibitor of bacteria proliferation. To test this hypothesis, we performed a colony forming unit (CFU) assay in order to quantitatively assess bacterial proliferation (Figure 7B). ORN178 and ORN208 were incubated with **NP1**-**NP3** prior to low speed centrifugation that selectively leads to the precipitation of bacteria-**NP** aggregates. Bacteria that remained in the supernatant were then seeded on LB-plates and incubated over-night to allow colony formation. Importantly, in contrast to ORN208, an about 10-fold reduction (90%) in colony formation was observed when ORN178 was incubated with **NP3**. Thus, the bacteria-**NP3** interaction is mannose specific, highly efficient and inhibits bacterial growth.

3. Conclusions

In this work we have reported a divergent approximation for the synthesis of different mannose-coated nanosytems with controlled topologies, without the need for multi-step oligosaccharide synthesis, by using a shot-gun like approach. The presence of a diyne group in the hydrophobic tail of the starting neoglycolipid allows the stabilization of the obtained nanomaterials by photopolymerization by a simple irradiation at 254 nm, with no need of any catalyst or initiator, facilitating the purification of the nanoparticles. 3D-static nanomicelles obtained by self-assembly and photopolymerization of the starting neoglycolipid have shown a dramatic (up to 40 fold) enhancement of the affinity toward ConA lectin as compared with methyl α-D-mannopyranoside as a monovalent control. The hierarchical self-assembly of neoglycolipid **2** on the hydrophobic surfaces of SWCNTs leads to the formation of stable, biocompatible, and water soluble glyconanoring-coated 1D-nanomaterial with a shish-kebab topology, **NP3**, that proved to be one of the best ConA binder reported to date, with a thousand time enhanced affinity in mannose molar basis. Notably, glyconanoring-coated carbon nanotubes efficiently and selectively regulate the agglutination and proliferation of the *E. coli* type 1 fimbriae. The simplicity of the approximation reported herein enables the modulation of the surface of the nanosystems for their application in anti-adhesive therapy to fight pathological events taking place through carbohydrate-lectin interactions. It is worth mentioning that, besides the advantages of having controlled size and topology, the mannose-coated 1D nanomaterial **NP3** can also benefit from the intact physical properties of SWCNTs. In this sense, well dispersed biocompatible single-walled carbon nanotubes are currently being actively investigated as nanovectors for smart delivery of bioactive molecules,[39] as composite in tissue engineering,[40] and thanks to their excellent ability to convert near infrared radiation into heat, as photothermal agent for hyperthermal ablation of tumors. In this sense, combining selective agglutination, growth inhibition of bacteria with heat generation, **NP3** hold great promise to annihilate pathogens and to bypass the problem of septic shock, one of the major actual treat.[41]

4 Experimental

4.1 General procedure for the synthesis of the nanoparticles

The synthesis, spectroscopic and characterization data of neoglycolipid **2**, are given in the supplementary material.

Dynamic micelles NP1: Neoglycolipid **2** (9 mg) was dissolved in milli-Q water (3.0 mL) above its critical micellar concentration determined by pyrene method. The clear solution was

sonicated with a sonication probe (125W output power) during 40 min at 5s ON/OFF intervals, in complete absence of light.

Static micelles NP2: Following the same procedure for the synthesis of **NP1**, and after 5 min, the obtained colloidal solution was subject to irradiation under a UV lamp at 254 nm for 1h, thus promoting the photo-polymerization of the di-yne functionalities into polymeric poly(diacetylene) derivatives.

Synthesis of NP3: In a typical experiment glycolipid **2** (1.0 mg) was dissolved in Milli-Q water (1.0 mL) above its critical micellar concentration. Then, SWCNTs (1.0 mg) purchased from Carbon Solutions Company (1-2 nm diameter; 0.5-1.5 mm length), were added and the mixture sonicated in an ultrasound bath for 1h. The resulting dark black precipitate (consisting in amorphous carbon and catalysts) was removed by low-speed centrifugation (825 x g, for 5 min) and decantation. The afforded stable black aqueous supernatant, composed by functionalized SWCNT/glycolipid **2**, was subject to irradiation under a UV lamp at 254 nm for 24h, thus promoting the photopolymerization of the diyne functionalities into the ring-shaped polymeric poly(diacetylene) derivatives around the SWCNT sidewalls. Subsequently, a second high-speed centrifugation of the solution (17968 x g, for 10 min) was accomplished, settling for this case, a black precipitated consisting in supramolecularly functionalized SWCNTs/glycolipid **1** (**NP3**) while glycolipid in excess remained in the supernatant. The centrifugation/decantation process was repeated four times, giving rise to pure **NP3** nanoconstructs.

4.2 Particles Size Measurement

The particle size and distribution of the micelles were measured using a Zetasizer Nano ZS system (Malvern Instruments). A laser beam at a wavelength of 632.8 nm was used. The scattering angle was set at 90º when measurements were conducted. The values are presented as the volume average size ± the standard deviation of three runs. The error in the measurements was calculated as the width at the mid height of the peak divided by two.

4.3 CMC Determination

The CMC of micelles were determined using pyrene as an extrinsic fluorescence probe. The pyrene concentration was maintained constant (0.6 10^{-6}M in THF), and the concentration of **2** was varied from 1 x 10^{-3} M to 0.5 x 10^{-6}. Fluorescence measurements were carried out at 25 ºC using a Varian Cary Eclipse spectrofluorometer. At the fixed excitation wavelength of 334 nm, the emission spectra were scanned from 300 to 350 nm. The fluorescence intensity ratios of pyrene at 339 and 335 nm (I339/I335, I1/I3) were calculated and plotted against the concentration logarithm of the neoglycolipid **2**. The CMC value was determined from the intersection of the two tangent lines; see Figure S2 in the supporting information.

4.4 TEM analyses

15 μL of a diluted solution of **NP1** or **NP2**, or a dispersion of glyconanotubes **NP3** were deposited on a carbon grid. Then 15 μL of a 2% uranyl acetate solution were added to negatively stain the nanoparticles, and the excess of liquid was removed by filter paper. TEM images were recorded on a Philips CM 10 or CM 200 apparatuses with an accelerating voltage of 80 kV or 200 kV.

4.5 AFM analysis

10 μL of diluted micelle solutions or **NP3** suspension were deposited on a just exfoliated mica grid (5 × 5 mm^2), and the excess of liquid was removed by filter paper. AFM images were taken by working on a tapping mode by Pico Plus Molecular Imaging, followed by a treatment with the WSxM 5.0 Develop 2.0 software.

4.6 Determination of carbohydrate quantity by anthrone method.

A freshly prepared solution of anthrone (0.5 % w/v in concentrated H_2SO_4, 1 mL) was added to various concentrations of D-mannose of known concentration (0.5 mL) under stirring in a water-bath. After that, the solution was then heated at 90ºC for 12 min. Then, the resulting green bluish solutions were rapidly cooled down in an ice bath during a further 10 min. Next, the absorbance of the solution was measured at 620 nm and the data were plotted against D-mannose concentrations, obtaining the calibration curve, see Figure S5 in the supporting information. To calculate the carbohydrate quantity on SWCNTs, 1.15 mg of **NP3** were dissolved in 0.5 mL Milli-Q water, and then a freshly prepared solution of anthrone was added, following the same procedure described above.

4.7. Enzyme-Linked Lectin Assay (ELLA).

In order to get information on the recognition of the mannosyl-coated nanosystems **NP1**, **NP2** and **NP3** by ConA, we performed enzyme-linked lectin assay (ELLA) experiments. This test measures the ability of a soluble saccharide to inhibit the association between a labelled lectin (here ConA lectin labeled with horseradish peroxidase, ConA-HRP) and a ligand immobilized on the microtiter well (here a yeast mannan). The presence of the relatively large HRP protein label (40 kD) prevents two lectin moieties from approaching each other, genrally resulting in 1:1 binding stoichiometries with the saccharide ligand. Methyl α-D-mannopyranoside was used as monovalent positive control to estimate the multivalent cluster effet.

Nunc-Inmuno™ plates (MaxiSorp™) were coated overnight with yeast (*Saccaromices cerevisae*) mannan at 100 μL/well diluted from a stock solution of 10 μg·mL^{-1} in 0.01 M phosphate buffer saline (PBS, pH 7.3 containing 0.1 mm Ca^{2+} and 0.1 mm Mn^{2+}) at room temperature. The wells were then washed three times with 300 μL of washing buffer (containing 0.05% (v/v) Tween 20) (PBST). The washing procedure was repeated after each of the incubations throughout the assay. The wells were then blocked with 150 μL/well of 1% BSA/PBS for 1 h at 37 ºC. After washing, the wells were filled with 100 μL of serial dilutions of horseradish peroxidase labelled concanavalin A lectin (ConA-HRP) from 10^{-1} to 10^{-5} mg mL^{-1} in PBS, and incubated at 37 ºC for 1 h. The plates were washed and 50 μL/well of 2,2'-azinobis-(3-ethylbenzothiazoline-6-sulfonic acid) diammonium salt (ABTS; 0.25 mg·mL^{-1}) in citrate buffer (0.2 m, pH 4.0 with 0.015% H_2O_2) was added. The reaction was stopped after 20 min by adding 50 μL/well of 1 m

H_2SO_4 and the absorbances were measured at 405 nm. Blank wells contained citrate-phosphate buffer. The concentration of lectin-enzyme conjugate that displayed an absorbance between 0.8 and 1.0 was used for inhibition experiments.

In order to carry out the inhibition experiments, each glyconanosystem or the control methyl α-D-mannopyranoside sample was added in a serial of 2-fold dilutions (60 μL/well) in PBS with 60 μL of the desired ConA-peroxidase conjugate concentration on Nunclon™ (Delta) microtiter plates and incubated for 1 h at 37 ºC. The above solutions (100 μL) were then transferred to the mannan-coated microplates, which were incubated for 1 h at 37 ºC. The plates were washed and the ABTS substrate was added (50 μL/well). Color development was stopped after 20 min and the absorbances were measured. IC_{50} values, assumed to be proportional to the corresponding binding affinities, were calculated from the percentages of inhibition with up to eleven different concentrations of each conjugate sample as follows:

% Inhibition = $(A_{(\text{no inhibitor})} - A_{(\text{with inhibitor})})/A_{(\text{no inhibitor})}$ x 100

Results in triplicate were used for the plotting the inhibition curves for each individual ELLA experiment. Typically, the IC_{50} values (concentration required for 50% inhibition of the Con A-yeast mannan association) obtained from several independently performed tests were in the range of ±12%. Nevertheless, the relative inhibition values calculated from independent series of data were highly reproducible.

4.8. Agglutination studies

Escherichia coli (*E. coli*) bacteria (ORN178 and ORN208 strains) were grown overnight at 30 ºC in LB medium with amphicilin in order to attain an optical density measured at 600 nm (OD_{600}) of approximately 1.0. The culture was centrifuged at 4500 rpm for 5 min. The supernatant was discarded and the pellet was suspended in Milli-Q water. Aliquots of bacterial cells (100 μL) were mixed with compounds analyzed (low and high concentration) and incubated at 4 ºC for 30 min with gentle shaking. After incubation, the mixture was centrifuged at 11,000 rpm for 5 min. The supernatant was discarded and the pellet was suspended, fixed in 2.5 % formaldehyde and observed under a wide-field fluorescence microscopy (DM-6000B, Leica) using N3 filter and a digital charge-coupled device camera (DFC350, Leica). Pictures were processed with LAS AF (Leica). Approximately 200 cells from at three independent experiments were analyzed for each strain.

4.9. Colony forming assay

Escherichia coli (*E.coli)* bacteria (ORN178 and ORN208 strains) were grown overnight at 30 ºC in LB medium with amphicilin in order to attain an optical density measured at 600 nm (OD_{600}) of approximately 5.0. The culture was centrifuged at 4500 rpm for 5 min. The supernatant was discarded and the pellet was suspended in Milli-Q water. Aliquots of dilution bacterial cells (100 μL) were mixed with the nanoparticles (low and high concentration) and incubated at 4 ºC for 30 min with gentle shaking. After incubation, the mixture was centrifuged at 1500 rpm for 2 min. The pellet was discarded and the supernatant was diluted by 10,000 fold to be evaluated. Petri plates were then incubated for 24 h at 30ºC, and the total number of colony-forming units (cfu) of plates was counted.

4.10. TEM analysis of bacterial agglutination.

After incubation of the nanoparticles with *E. coli* for 2 h., the aggregates were fixed by formaldehyde treatment and washed with PBS. 20 μL of the solution were then deposited on a copper grid coated with a carbon film, and the excess of liquid removed by filter paper. TEM images were obtained with a Philips CM 10 apparatus with an accelerating voltage of 80 kV.

Acknowledgements

Financial support was provided by the Andalusian Ministry of Economy, Science and Innovation (P07-FQM-2774 to NK, P11-FQM-8046 to IF, FQM-1467 to JMGF, P08-CTS-04297, and P11-CTS-7962 to REW), the PAIDI Program from the Andalusian Government (FQM-313 to NK, FQM-102 to IF, BIO-026 to REW), the Spanish Ministry of Economy and Competitiveness (CTQ2013-49066-C2-1-R to NK and SAF2013-44021R to EMSF) and the European Union Seventh Framework Programme (FP7-People-2012-CIG, grant agreement no. 333594 to EMSF). The European Regional Development Fund (FEDER) and the European Social Fund (ESF) are also acknowledged. MA was recipient of a MAEC-AECID PhD fellowship. JJC was recipient of a JAE-CSIC postdoctoral fellowship. EFG is recipient of a fellowship from the Junta de Andalucia. We thank the Centre of Research Technology and Innovation of the University of Seville (CITIUS) for the use of TEM, AFM, and NMR facilities.

Notes and references

1 a) D. B. Werz, P. H. Seeberger, *Chem. Eur. J.* 2005, **11**, 3194 – 3206. b) S. Bhatia, M. Dimde, R. Haag, *Med. Chem. Commun*., 2014, **5**, 862–878. c) R. D. Astronomo, D. R. Burton, *Nature Rev. Drug Discovery* 2010, **9,** 308-324. d) J. E. Hudak, C. R. Bertozzi, *Chem. Biol.* 2014, **21***,* 16-37.

2 D. H Dube, C. R. Bertozzi, *Nature Rev. Drug Discovery* 2005, **4,** 477-488. b) C. R. Bertozzi, L. L. Kiessling, *Science* 2001, **293**, 2357-2364. c) R. S. Haltiwanger, J. B. Lowe, *Annu. Rev. Biochem.* 2004, **73***,* 491-537. d) Y. van Kooyk, G.A. Rabinovich, *Nat. Immunol*., 2008, **9**, 593−601. e) R.G. Spiro, *Glycobiology*, 2002, **12**, 43R−56R.

3 a) W. Weis, H. Brown, S. Cusak, J. J. Skehel, D. C. Wiley, *Nature,* 1988, **333**, 426-431. b) J. C. PJ. S. Gamblin, J. J. Skehel, *J. Biol. Chem*. 2010, **285**, 28403-28409.

4 J. S. McLellan, M. Pancera, C. Carrico, J. Gorman, J.-P. Julien, R. Khayat, R. Louder, R. Pejchal, M. Sastry, K. Dai, S. O'Dell, N. Patel, S. Shahzad-ul-Hussan, Y. Yang, B. Zhang, T. Zhou, J. Zhu, J. C. Boyington, G.-Y. Chuang, D. Diwanji, I. Georgiev, Y. D. Kwon, D. Lee, M. K. Louder, S. Moquin, S. D. Schmidt, Z.-Y. Yang, M. Bonsignori, J. A. Crump, S. H. Kapiga, N. E. Sam, B. F. Haynes, D. R. Burton, W. C. Koff, L. M.Walker, S. Phogat, R. Wyatt, J. Orwenyo, L.-X. Wang, J. Arthos, C. A. Bewley, J. R. Mascola, G. J. Nabel, W. R. Schief, A. B. Ward, I. A. Wilson, P. D. Kwong, *Nature,* 2011, **480***,* 336-343.

5 M. Brudner., M. Karpel., C. Lear, L. Chen, L. M. Yantosca, C. Scully, A. Sarraju, A. Sokolovska, M. R. Zariffard, D. P. Eisen, B. A. Mungall, D. N. Kotton, A. Omari, I-C. Huang, M. Farzan, K. Takahashi, L. Stuart, G. L. Stahl, A. B. Ezekowitz, G. T. Spear, G. G. Olinger, E. V. Schmidt, I: C. Michelow, *Plos One* 2013, **8**, e60838.

6 a) B. Lepenies, J. Lee, S. Sonkaria, *Adv. Drug Delivery Rev.* 2013, **65**, 1271-1281. b) T. B. Geijtenbeek, D. S. Kwon, R. Torensma, S. J. van Vliet, G. C. van Duijnhoven, J. Middel, I. L. Cornelissen, H. S. Nottet, V. N. KewalRamani, D. R. Littman,

C. G. Figdor, Y. van Kooyk, *Cell* 2000, **100**, 587-597. c) M. Sanchez-Navarro, J. Rojo, *Drug News Perspect.* 2010, **23**, 557-572.

7 a) T. K. Lindhorst, *Top. Curr. Chem.* 2002, **218**, 201. b) R. J. Peters, *Med. Res. Rev.* 2007, **27**, 796-816. c) N. Parera Pera, R. J. Peters, *Med. Chem. Commun.* 2014, **5**, 102-1035. d) A. Bernardi, J. Jimenez-Barbero, A. Casnati, C. De Castro, T. Darbre, F. Fieschi, J. Finne, H. Funken, K. Jaeger, M. Lahmann, T. K. Lindhorst, M. Marradi, P. Messner, A. Molinaro, P. V. Murphy, C. Nativi, S. Oscarson, S. Penades, F. Peri, R. J. Pieters, O. Renaudet, J. Reymond, B. Richichi, J. Rojo, F. Sansone, C. Schaeffer, W. B. Turnbull, T. Velasco-Torrijos, S. Vidal, S. Vincent, T. Wennekes, H. Zuilhof and A. Imberty, *Chem. Soc. Rev*., 2013, **42**, 4709-4727.

8 a) N. Sharon, *Biochim. Biophys. Acta* 2006, **1760**, 527–537. b) I. Ofek, D. L. Hasty, N. Sharon, *FEMS Immunol. Med. Microbiol.* 2003, **38**, 181-191. c) C. Bavington, C. Page, *Respiration* 2005, **72**, 335-344. A. M. Krachlera, K. Orthb, *Virulence* 2013, **4**, 284-294.

9 a) D. J. Payne, M. N. Gwynn, D. J. Holmes, D. L. Pompliano, *Nature Rev. Drug Discov.* 2007, 29-40. b) K. Bush, P. Courvalin, G. Dantas, J. Davies, B. Eisenstein, P. Huovinen, G. A. Jacoby, R. Kishony, B. N. Kreiswirth, E. Kutter, S. A. Lerner, S. Levy, K. Lewis, O. Lomovskaya, J. H. Miller, S. Mobashery, L. J. Piddock, S. Projan, C. M. Thomas, A. Tomasz, P. M. Tulkens, T. R. Walsh, J. D. Watson, J. Witkowski, W. Witte, G. Wright, P. Yeh, H. I. Zgurskaya, *Nature Rev. Microbiol.* 2011, **9**, 894-896.

10 a) T. J. Boltje, T. Buskas, G.-J. Boons, *Nat. Chem.* 2009, **1**, 611-622. b) B. Lepenies, J. Yin, P. H. Seeberger, *Curr. Opin. Chem. Biol.* 2010, **14**, 404–411. c) X. Zhu, R. R. Schmidt, *Angew. Chem. Int. Ed. Engl*. 2009, **48**, 1900–1934.

11 a) A. Varki, *Glycobiology* 1993, **3**, 97. b) R. A. Dwek, *Chem. Rev.* 1996, **96**, 683. c) R. J. Peters, *Org. Biomol. Chem.* 2009, **7**, 2013.

12 a) C.R. Becer, *Macromol. Rapid Commun*., 2012, **33**, 742–752. b) D. Deniaud, K. Julienne, S.G. Gouin. *Org. Biomol. Chem*., 2011, **9**, 966–979. c) J.J. Lundquist, E.J. Toone. *Chem. Rev.,* 2002, **102**, 555–578.

13 a) Y. C. Lee, R. T. Lee, *Acc. Chem. Res*. 1995, **28**, 321. b) L. Baldini, A. Casnati, F. Sansone, R. Ungaro, *Chem. Soc. Rev*. 2007, **36**, 254. c) A. Dondoni, A. Marra, *Chem. Rev*. 2010, **110**, 4949. d) A. Kiviniemi, P. Virta, M. S. Drenichev, S. N. Mikhailov, H. Lonnberg, H. *Bioconjugate Chem*. 2011, **22**, 1249. e) M. Durka, K. Buffet, J. Iehl, M. Holler, J. F. Nierengarten, S. P. Vincent, *Chem. Eur. J.* 2012, **18**, 641. e) Y. M. Chabre, R. Roy, *Curr. Top. Med. Chem.* 2008, **8**, 1237-1285. f) M. Marradi, Chiodo, I. Garcia, S. Penades, *Chem. Soc. Rev.* 2013, **42**, 4728-4745. g) C. R. Becer, *Macromol. Rapid Commun.* 2012, **33**, 742-752.

14 a) S. M. Dimick, S. C. Powell, S. A. McMahon, D. N. Moothoo, J. H. Naismith, E. J. Toone, *J. Am. Chem. Soc.* 1999, **121**, 10286. b) M. K. Müller, L. Brunsveld, *Angew. Chem., Int. Ed.* 2009, **48**, 2921. c) D. Deniaud, K. Julienne, S. G. Gouin, *Org. Biomol. Chem.* 2011, **9**, 966. d) D.-W. Lee, T. Kim, I.-S. Park, Z. Huang, M. Lee, *J. Am. Chem. Soc.* 2012, **134**, 14722. e) G. Yu, Y. Ma, C. Han, Y. Yao, G. Tang, Z. Mao, C. Gao, F. Huang, *J. Am. Chem. Soc.* 2013, **135**, 10310-10313. f) G. Yu, J. Li, W. Yu, C. Han, Z. Mao, C. Cao, F. Huang, *Adv. Mater.* 2013, **25**, 6373-6379. g) E. L. Dane, A. E. Ballok, G. A. O'Toole, M. W. Grinstaff, *Chem Sci.,* 2014, **5**, 551-557.

15 a) G. M. Whitesides, J. P. Mathias, C. T. Seto, *Science*, 1991, **254**, 1312-1319. b) J. M. Lehn, *Proc. Natl. Acad. Sci. USA* 2002, **99**, 4763-4768. c) J. M. Lehn, *Science* 2002, **295**, 2400-2403. d) G. M. Whitesides, *Small* 2005, **1**, 172-179. e) Y. –B. Lim, K.-S. Moon, M. Lee, *Chem. Soc. Rev.,* 2009, **38**, 925-934. f) H. Otsuka, *Adv. Drug Delivery Rev.* 2003, **55**, 403-419. g) D. W. Pack, A. S. Hoffman, S. Pun, P. S. Stayton, *Nat. Rev. Drug Discov.,* 2005, **4**, 581-593. h) Y. He, T. Ye, M. Su, C. Zhang, A. E. Ribbe, W. Jiang, C. Mao, *Nature,* 2008, **452**, 198-201.

16 a) Barnard, A.; Smith,D. K. *Angew. Chem., Int. Ed.,* 2012, **51**, 6572-6581. b) Badjic, J. D.; Nelson, A.; Cantrill, S. J.; Turnbull, W. B.; Stoddart, J. F. *Acc. Chem. Res.* 2005, **38**, 723-732. c) Levine, P. M.; Carberry, T. P.; Holubb, J. M.; Kirshenbaum, K. *Med. Chem. Commun.*, 2013, **4**, 493-509. d) D. A. Uhlenheuer, K. Petkau, L. Brunsveld, *Chem. Soc. Rev.,* 2010, **39**, 2817–2826. e) Petkau-Milroy, K.; Brunsveld, L. *Org. Biomol. Chem.* 2013, **9**, 219-232.

17 a) Reppy, M. A.; Pindzola, B. A. *Chem. Commun.,* 2007, 4317-4388. b) Lauher, J. W.; Fowler, F. W.; Goroff, N. S. *Acc. Chem. Res.,* 2008, **41**, 1215-1229. c) Yoon, B.; Lee, S.; Kim, J.-M. *Chem. Soc. Rev.,* 2009, **38**, 1958-1968. d) Sun, X.; Chen, T.; Huang, S.; Li, L.; Peng, H. *Chem. Soc. Rev.* 2010, **39**, 4244-4257. e) Yarimaga, O.; Jaworski, J.; Yoon, B.; Kim, J.-M. *Chem. Commun.* 2012, **48**, 2469-2485.

18 a) R. H. Baughman, A. A. Zakhidov, W. A. C. de Heer, *Science* 2002, **297**, 787-792. b) M. F. L. De Volder, S. H. Tawfick, R. H. Baughman, A. J. Hart, *Science* 2013, **339**, 535-539.

19 a) K. Khiar, M. Pernía-Leal, R. Baati, C. Ruhlmann, C. Mioskowski, P. Schultz, I. Fernández, I.; *Chem. Commun*. 2009, 4121-4123. b) M. Assali, J. –J. Cid, M. Pernía-Leal, M. Muñoz-Bravo, I. Fernández, N Khiar, *ACS Nano*, 2013, **7**, 2145-2153.

20 M. Assali, J.-J. Cid; I. Fernández, N. Khiar, *Chem. Mater*. 2013, **25**, 4250-4261.

21 a) S. Ceccioni, S. Faure, U. Darbost, I. Bonnamour, H. Parrot-Lopez, O. Roy, C. Taillefumier, M. Wimmerová, J.-P. Praly, A. Imberty, S. Vidal, *Chem. Eur. J.* 2011, **17**, 2146-2159. b) Y. Brissonet, C. Ortiz Mellet, S. Morandat, M. I. García Moreno, D. Deniaud, S. E. Mattews, S. Vida, S. Sesták, K. El Kirat, S. G. Gouin, *J. Am. Chem. Soc.* 2013, **135**, 18427-18435. c) D.-W. Lee, T. Kim, I-S. Park, Z. Huang, M. Lee, J. Am. Chem. Soc. 2012, 134, 14722-14725. d) J.-H. Ryu, E. Lee, Y.-b, Lim, M. Lee, *J. Am. Chem. Soc.* 2007, **129**, 4808. e) J. E. Gestwicki, L. E. Strong, C. W. Cairo, F. J. Boehm, L. L. Kiessling, *Chem. Biol*. 2002, **9**, 163. f) L. Gu, T. Elkin, X. Jian, H. Li, Y. Lin, L. Qu, T. R. J. R. Joseph, Y.-P. Sun, *Chem. Commun*. 2005, 874.

22 a) C.-W. Li, K.-W. Hon, B. Ghosh, P. H. Li, H.-Y. Lin, P.-H. Chan, C.-H. Lin, Y.-C. Chen, K.-K T. Mong, *Chem. Asian J.* 2014, **9**, 1786-1796. b) T. Kim, H. Lee, Y. Kim, J.-M. Namb, M. Lee, *Chem. Commun*. 2013, **49**, 3949-3951. c) K.-R. Wang, Y.-Q. Wang, H.-W. An, J.-C. Zhang, X.-L. Li, *Chem. Eur. J.* 2013, **19**, 2903-2909. d) R. Su, L. Li, X. Chen, J. Han, S. Han, *Org. Biomol. Chem*. 2009, **7**, 2040-2045. e) J.-E. Gestwicki, C. W. Cairo, L. E. Strong, K. A. Oetjen, L. L. Kiessling, *J. Am. Chem. Soc*. 2002, **124**, 14922-14933.

23 M. Hartmann, T. K. Lindhorst, *Eur. J. Org. Chem.* 2011, 3583-3609.

24 G. B. Ray, I. Chakraborty, S. P. Moulik, *J. Coll. Interf. Sc.* 2006, **294**, 248-254.

25 M. Pernía Leal, M. Assali, J. J. Cid, V. Valdivia, J. M. Franco, I. Fernández, D. Pozo and N. Khiar, *Nanoscale,* 2015, DOI: 10.1039/c5nr05956a

26 M. A. Jermyn, *Anal. Biochem.* 1975, **68**, 332-335.

27 H. Bittiger, H. P. Schnebli, *Concanavalin A as a Tool*, Wiley, 1976.

28 P. N. Kanellopoulos, K. Pavlou, A. Perrakis, B. Agianian, C. E. Vorgias, C. Mavrommatis, M. Soufi, P. A. Tucker, S. J. Hamodrakas, *J. Struct. Biol*. 1996, **116**, 345-355.

29 a) J. J. Lundquist, E. J. Toone, *Chem. Rev.* 2002, **102**, 555–578. b) D. Deniaud, K. Julienne, S. G. Gouin, *Org. Biomol. Chem*. 2011, **9**, 966-979.

30 a) T. K. Lindhorst, S. Kötter, J. Kubisch, U. Krallmann-Wenzel, S. Ehlers, V. Kren, *Eur. J. Org. Chem.* 1998, 1669-1674. b) J. B. Corbell, J. J. Lundquist, E. J. Toone, *Tetrahedron: Asymmetry* 2000, **11**, 95-111. c) K. Petkau-Milroy, Luc Brunsveld, *Eur. J.*

Org. Chem. 2013, 3470-3476. d) B. Trastoy, D. A. Bonsor, M. E. Pérez-Ojeda , M. L. Jimeno, A. Méndez-Ardoy, J. M. García Fernández, E. J. Sundberg, J. L. Chiara, *Adv. Funct. Mater.* 2012, **22**, 3191-3201.

31 L. L. Kiessling, J. E. Gestwicki, L. E. Strong, *Angew. Chem. Int. Ed.* 2006, **45**, 2348-2368.

32 A. Siriwardena, M. Khanal, A. Barras, O. Bande, T. Mena-Barragán, C. Ortiz Mellet, J. M. Garcia Fernández, R. kherroub and S. Szunerits, *RSC Adv.* 2015, **5**, 100568.

33 T. K. Dam, C. F. Brewer, *Biochemistry,* 2008, **47**, 8470-8476. V. Witmann, R. Peters, *Chem. Soc. Rev.,* 2013, **42**, 4492-4503

34 a) D. Choudhury, *Science* 1999, **285**, 1061-1066. b) P. Klemm, L. Hjerrild, M. Gjermansen and M. A. Schembri, *Mol. Microbiol*., 2004, **51**, 283-296.

35 a) P. Klemm, L. Hjerrild, M. Gjermansen and M. A. Schembri, *Mol. Microbiol*., 2004, **51**, 283-296. b) I. Adlerberth, L. A. Hanson, C. Svanborg, A. M. Svennerholm, S. Nordgren and A. E. Wold, *Microb. Pathog.* 1995, **18**, 373-385. c) C. S. Eden and H. A. Hansson, *Infect. Immun*. 1978, **21**, 229-237. d) C. G. Korea, R. Badouraly, M. C. Prevost, J. M. Ghigo, C. Beloin, *Environ. Microbiol*. *2010*, **12**, 1957-1977. e) E. V. Sokurenko, M. A. Schembri, E. Trintchina, K. Kjaergaard, D. L. Hasty and P. Klemm, *Mol. Microbiol*. 2001, **41**, 675-686. f) S. Tardito, I. Bassanetti, C. Bignardi, L. Elviri, M. Tegoni, C. Mucchino, O. Bussolati, R. Franchi-Gazzola, L. Marchio, *J. Am. Chem. Soc.* 2011, **133**, 6235-6242. g) R. Virkola, *FEMS Microbiol. Lett.* 1987, **40**, 257-262. h) X. R. Wu, T. T. Sun and J. J. Medina, *Proc. Natl. Acad. Sci. U. S. A*. 1996, **93**, 9630-9635.

36 a) X. R. Wu, T. T. Sun and J. J. Medina, *Proc. Natl. Acad. Sci. U. S. A*., 1996, **93**, 9630–9635. b) S. L. Chen, C. S. Hung, J. S. Pinkner, J. N. Walker, C. K. Cusumano, Z. Li, J. Boukaert, J. I. Gordon, S. J. Hultgren, *Proc. Natl. Acad. Sci. U. S. A*., 2009, **106**, 2243-22444.

37 S. L. Harris, P. A. Spears, E. A. Havell, T. S. Hamrick, J. R. Horton, P. E. Orndorff *J. Bacteriol.* 2001, **183**, 4099-4102.

38 a) Y. Lim, S. Park, E. Lee, J. H. Ryu, Y. R. Yoon, T. H. Kim, M. Lee, *Chem. Asian J.* 2007, **2**, 1363. b) Y. Lim, S. Park, E. Lee, H. Jeong, J. H. Ryu, M. S. Lee, M. Lee, *Biomacromolecules* 2007, **8**, 1404. c) H. Wang, L. Gu, Y. Lin, F. Lu, M. J. Meziani, P. G. Luo, P. G.; W. Wang, L. Cao, Y. P. Sun, *J. Am. Chem. Soc.* 2006, **128**, 13364. d) P. G. Luo, H. Wang, L. Gu, F. Lu, Y. Lin, K. A. Christensen, S. T. Yang, Y. P. Sun, *ACS Nano* 2009, **3**, 3909. e) L. Gu, T. Elkin, X. Jiang, H. Li, L. Qu, T-R. J. Tzeng, R. Joseph, Y. P. Sun. *Chem Commun.* 2005, 874-876

39 J. Chen, S. Chen, X. Zhao, L. V. Kuznetsova, S. S. Wong, I. Ojima, *J. Am. Chem. Soc.* 2008, **130**, 16778-16785. b) S. Dhar, Z. Liu, J. Thomale, H. Dai, S. J. Lippard, *J. Am. Chem. Soc.* 2008, **130**, 11467-11476. c) Z. Liu, X. Sun, N. Nakayama-Ratchford, H. Dai, *ACS Nano* 2007, **1**, 50-56.Z. d) Z. Liu, K. Chen, C. Davis, S. Sherlock, Q. Cao, X. Chen, H. Dai, *Cancer Res*. 2008, **68**, 6652-6660. e) Z. Zhang, X. Yang, Y. Zhang, B. Zeng, S. Wang, T. Zhu, R. B. Roden, Y. Chen, R. *Clin Cancer Res.* 2006, **12**, 4933-4939. f) J. E. Podesta, K. T. Al-Jamal, M. A. Herrero, B. Tian, H. Ali-Boucetta, V. Hegde, A. Bianco, M. Prato, K. Kostarelos, *Small* 2009, **5**, 1176-1185.

40 a) S. R. Shin, H. Bae, J. M. Cha, J. Y. Mun, Y.-C. Chen, H. Tekin, H. Shin, S. Farshchi, M. R. Dokmeci, S. Tang, A. Khademhosseini. A. *ACS Nano* 2012, ***6***, 362. b) S. R. Shin, S.M. Jung, K. Zalabany, K. Kim, P. Zorlutuna, S. B. Kim, M. Nikkhah, M. Khabiry, M Azize, J. Kong, K.-T. Wan, T. Palacios, M. R. Dokmeci, S. Tang, A. Khademhosseini. *ACS Nano* 2013, **7**, 2369-2380.

41 a) R. Singh, S. V. Torti, *Adv. Drug Delivery Rev*. 2013, **65**, 2045–2060. b) P. C. Ray, S. A. Khan, A. K. Singh, D. S. Senapti, Z. Fan, *Chem Soc. Rev.* 2012, **41**, 3193-3209.

Graphical Abstract

Acting as veritable glue, 1D-coated mannose carbon nanotubes efficiently and selectively regulate the agglutination and proliferation of the enterobacteria *Escherichia coli* type 1 fimbriae, much better than mannose coated 3D-micelles.